A universal microfluidic approach for integrated analysis of temporal homocellular and heterocellular signaling and migration dynamics

Biosensors and Bioelectronics 211 (2022) 114353

Contents lists available at ScienceDirect

Biosensors and Bioelectronics

journal homepage: www.elsevier.com/locate/bios

A universal microfluidic approach for integrated analysis of temporal homocellular and heterocellular signaling and migration dynamics

Haowen Yang [a,b], Nidhi Sinha [a,b], Ulfert Rand [c], Hansjörg Hauser [c], Mario Köster [c], Tom F.A. de Greef [b,d], Jurjen Tel [a,b,*]

[a] Laboratory of Immunoengineering, Department of Biomedical Engineering, Eindhoven University of Technology, Eindhoven, 5600MB, the Netherlands
[b] Institute for Complex Molecular Systems, Eindhoven University of Technology, Eindhoven, 5600 MB, the Netherlands
[c] Model Systems for Infection and Immunity, Helmholtz Centre for Infection Research, 38124, Braunschweig, Germany
[d] Computational Biology Group, Department of Biomedical Engineering, Eindhoven University of Technology, 5600MB, Eindhoven, the Netherlands

ARTICLE INFO

Keywords:
Microfluidics
Cellular signaling
Single-cell analysis
Dynamic stimulation
STAT dynamics
Cell migration

ABSTRACT

Microfluidics offers precise and dynamic control of microenvironments for the study of temporal cellular responses. However, recent research focusing solely on either homocellular (single-cell, population) or heterocellular response may yield insufficient output, which possibly leads to partial comprehension about the underlying mechanisms of signaling events and corresponding cellular behaviors. Here, a universal microfluidic approach is developed for integrated analysis of temporal signaling and cell migration dynamics in multiple cellular contexts (single-cell, population and coculture). This approach allows to confine the desired number or mixture of specific cell sample types in a single device. Precise single cell seeding was achieved manually with bidirectional controllability. Coupled with time-lapse imaging, temporal cellular responses can be observed with single-cell resolution. Using NIH3T3 cells stably expressing signal transducer and activator of transcription 1/2 (STAT1/2) activity biosensors, temporal STAT1/2 activation and cell migration dynamics were explored in isolated single cells, populations and cocultures stimulated with temporal inputs, such as single-pulse and continuous signals of interferon γ (IFNγ) or lipopolysaccharide (LPS). We demonstrate distinct dynamic responses of fibroblasts in different cellular contexts. Our presented approach facilitates a multi-dimensional understanding of STAT signaling and corresponding migration behaviors.

1. Introduction

Mammalian cells constantly discern and handle myriads of time-varying environmental perturbations. Individual cells constantly integrate a multitude of extracellular inputs to trigger complex signaling networks (Osborn and Olefsky, 2012; Purvis and Lahav, 2013), and generate heterogeneous outputs (Spiller et al., 2010). Interesting outputs, such as Extracellular signal-regulated kinase (ERK) (Lavoie et al., 2020), nuclear factor kappa B (NF-κB) (Dorrington and Fraser, 2019), and signal transducer and activator of transcription (STAT) (Villarino et al., 2017), have been uncovered from cellular signaling investigation in either homocellular (single-cell (Junkin and Tay, 2014), population (Bennett and Hasty, 2009)) or heterocellular (Oyler-Yaniv et al., 2017) context (Fig. 1A and B). However, the insufficient output, from single context, possibly leads to partial comprehension about the underlying mechanisms of signaling activities. For instance, interferon α (IFNα) secretion dramatically decreased in droplet-isolated single plasmacytoid dendritic cells (pDCs) in comparison with a population of pDCs (Wimmers et al., 2018). Several inflammatory cytokines were either up- or down-regulated in macrophage/fibroblast co-cultures compared to monocultured cells (Holt et al., 2010). Thus, observing cellular events in multiple contexts becomes crucial for multi-dimensional understanding of signaling process.

Taking advantage of precise environmental control, microfluidic techniques have been applied to investigate homocellular (single-cell (Junkin et al., 2016), population (Bennett and Hasty, 2009; Tay et al., 2010)) or heterocellular signaling (Sakthivel et al., 2019). The designs for single-cell analysis typically rely on special geometric structures (Pang et al., 2020), such as pillar-like (Junkin et al., 2016) and V-type valves (Rho et al., 2016), which are only applicable to cells with specific

* Corresponding author. Laboratory of Immunoengineering, Department of Biomedical Engineering, Eindhoven University of Technology, Eindhoven, 5600MB, the Netherlands.
E-mail address: j.tel@tue.nl (J. Tel).

https://doi.org/10.1016/j.bios.2022.114353
Received 17 March 2022; Received in revised form 26 April 2022; Accepted 6 May 2022
Available online 11 May 2022

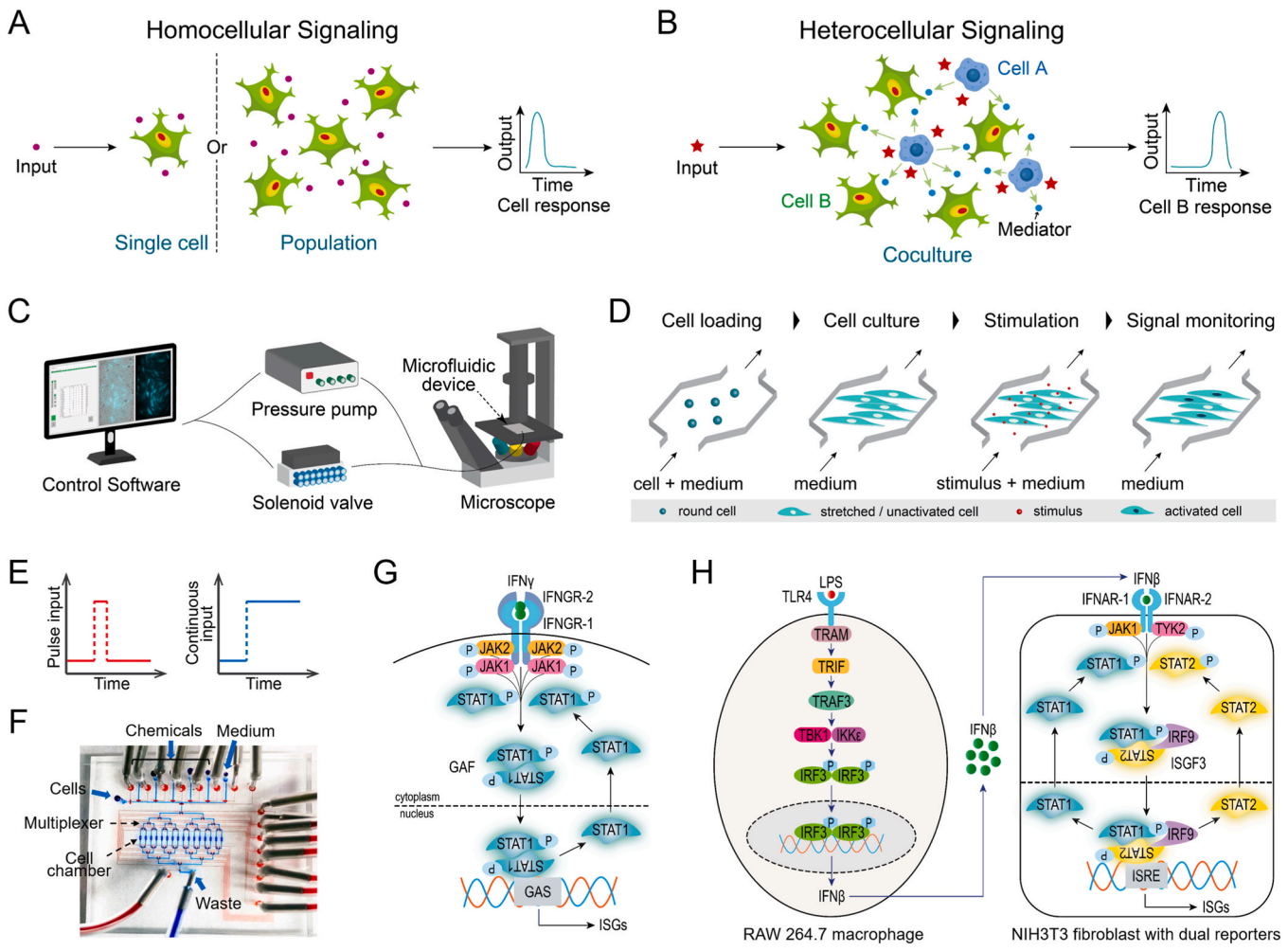

Fig. 1. (A) Homocellular signaling scenario: an environmental input like cytokines are detected and processed by a responding single cell or a group of identical cells, and then are transformed into an output (e.g., signaling factor activity and cell migratory behavior). (B) Heterocellular signaling scenario: an original input like a bacterial stimulus induces secretion of mediators (e.g., cytokines) in one cell type (cell A, e.g., macrophage), and then their heterotypic neighbors (cell B, e.g., fibroblast) transform the mediator signals into a final output. (C) The entire system built in this study. The delivery of defined input types (e.g., pulse, continuous) are controlled by a pressure pump and solenoid valves. Outputs are acquired via time-lapse live-cell microscopy. (D) The workflow to measure the activities of transcription factors in living cells with fluorescence reporters using our microfluidic platform. (E) Two input profiles used in this study. (F) The multilayer microfluidic device with control layer in red (e.g., microvalves) and flow layer in blue (e.g., cell chambers). (G) Schematics of IFNγ-mediated STAT signaling pathway (Michalska et al., 2018). Nucleocytoplasmic shuttling of STAT1 is initiated upon IFNγ stimulation. (H) Schematics of heterocellular signaling between macrophage and fibroblast. Lipopolysaccharide (LPS) first induces IFNβ secretion in RAW 264.7 macrophage. IFNβ, as a signaling mediator, is subsequently propagated to trigger nucleocytoplasmic shuttling of STAT1 and STAT2 in NIH3T3 fibroblast. The dynamics of STAT1 and STAT2 can be measured via their CFP and YFP reporters.

size and requires considerate optimization efforts. The microfluidic devices used to study heterocellular signaling are usually utilized to coculture heterotypic cell types in two separate microchambers connected by microchannels (Rothbauer et al., 2018; Vu et al., 2017). As a result, the cell-specific signaling data from the non-contacting coculture may under-represent the influence of heterocellular signaling within a mixture of heterotypic cells (Tape, 2016; Wells and Wiley, 2018). Although it has become possible to study either homocellular (single-cell, population) or heterocellular signaling on different specialized microfluidic platforms, performing this study on a single platform remains a great challenge due to the limitation of special structure designs for each condition.

Here we present a universal microfluidic strategy enabling multi-perspective study of temporal dynamics in multiple cellular contexts. We controllably confined single cells, populations, and cocultures in a single trap-free device, and delivered input signals with high precision (Fig. 1C–F). Coupled with live-cell imaging, we can study homocellular (single-cell, population) and heterocellular signaling with single-cell resolution, in addition to the cell migratory behaviors. Given that temporal STAT1/2 activities (Fig. 1G and H) remain poorly understood, we herein applied our approach to investigate the STAT1/2 responses in multiple cellular contexts (i.e., single-cell, population and coculture). Temporal stimulation profiles, such as one-pulse and continuous IFNγ or lipopolysaccharide (LPS) was implemented to induce STAT activation in NIH3T3 fibroblasts (Fig. 1G and H). We demonstrate the establishment of homocellular (single-cell, population) and heterocellular signaling architectures in one single device.

2. Results and discussion

2.1. Cell seeding and culture in the microfluidic device

By delivering gradient concentrations of cell sample, we confined the gradient density of cells in each chamber (Fig. 2A, B and S6A, B). For coseeding, different cell combinations in each chamber can be realized by delivering cell sample at specific mixture ratios (Fig. 2C). We observed higher successful rates at macrophage:fibroblast (M:F) ratios 10:1, 1:10 and 1:1 than at 3:1 and 1:3 (Fig. 2D and E). In particular, we,

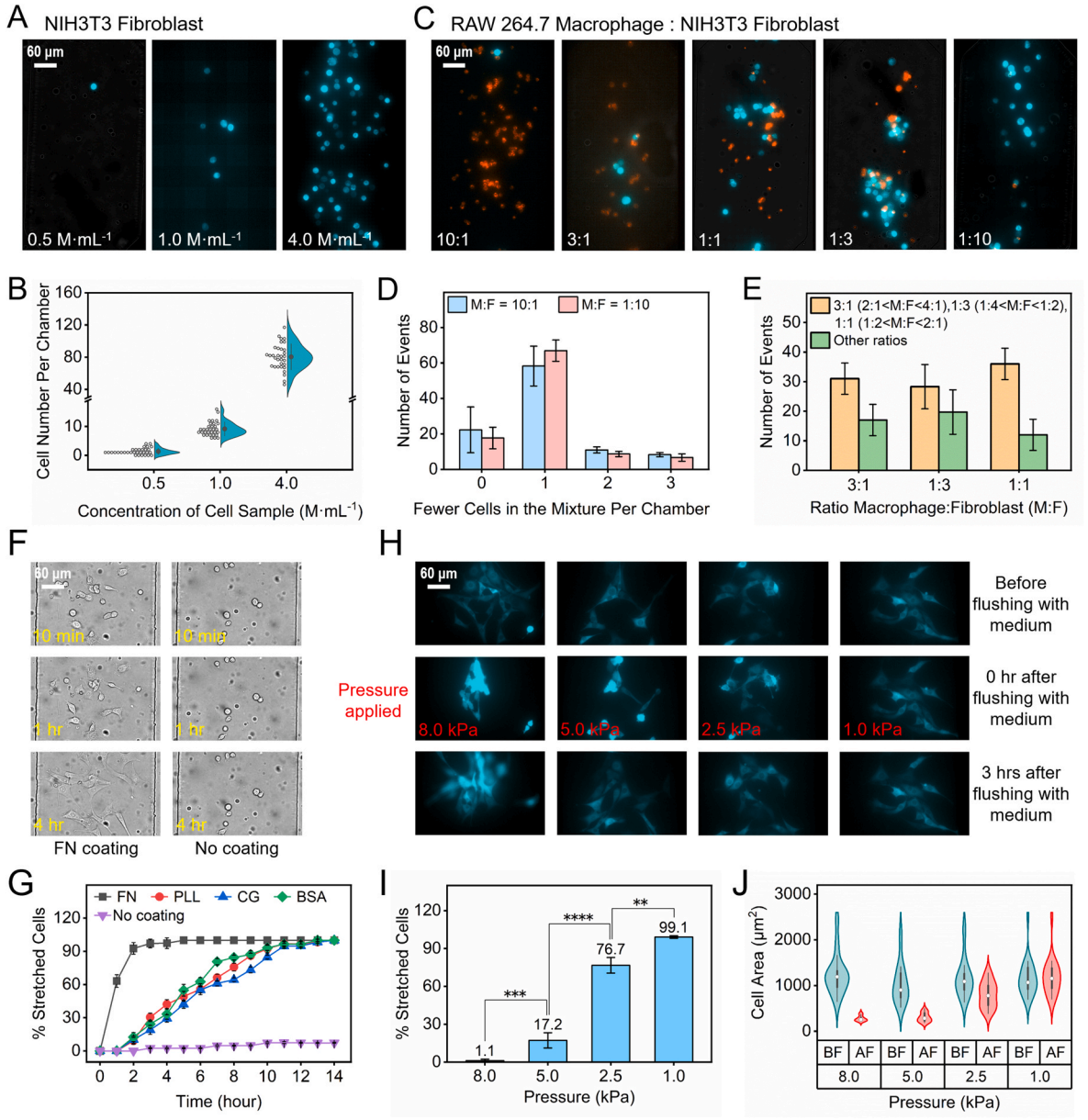

Fig. 2. (A) Monoseeding of NIH3T3 fibroblasts in each microfluidic chamber by delivering concentrations of cell suspension ranging from 0.5 to 4 million·mL^{-1} (M·mL^{-1}). (B) Correlation between the number of seeded cells in one chamber and the cell sample concentration. (C) The proportion of macrophage/fibroblast in each chamber after coseeding cell mixture at a macrophage/fibroblast (M:F) ratio 10:1, 3:1, 1:1, 1:3, or 1:10. (D) The frequency of fewer cells of one type with respect to the other cell type in the mixture after coseeding at a M:F ratio 10:1 or 1:10. (E) The frequency of M:F ratio 3:1, 1:3 or 1:1 in each chamber after coseeding with corresponding ratio. (F) Fibroblasts gradually stretch on fibronectin-coated surface but do not stretch on the substrate with no coating. (G) Cell stretching dynamics with different cell adhesion molecules (FN: fibronectin, PLL: poly-L-lysine, CG: collagen, BSA: bovine serum albumin, No coating: the substrate was not coated with any adhesion molecule). (H) Characteristics of cell morphology variation before and after flushing medium under different pressures. (I) Correlation between the percentage of stretched cells and the applied pressures. Error bars indicate SD. Means with significant differences were determined by Student *t*-test; $^{**}p < 0.01$, $^{***}p < 0.001$, $^{****}p < 0.0001$. Data are representative of three independent experiments. (J) The influence of variable pressures on cell areas. BF: before flushing medium, AF: after flushing medium.

alternatively, implemented single cell seeding manually using a 1 mL syringe instead of the Fluigent pump (Figs. S7A and B). With bidirectional control, the hand control strategy enables precise single cell confinement (Fig. S7C). The fibronectin-coated chambers allowed single cells to spread (Fig. S8). Although Junkin, M. et al. showed single macrophage confinement with pilar-like traps, those adherent cells were likely to partially attach and spread on the vertical surface of traps (Fig. S9A) (Junkin et al., 2016). This may affect image-based quantitative analysis for nuclear localization of signaling proteins (Fig. S9B). With hydrodynamic shuttling chips, single cells can be trapped and released into isolated chambers, allowing single cells to spread on the flat substrate (He et al., 2019; Hong et al., 2012). However, short-term signals such as pulsed inputs become difficult to control. Thus, our microfluidic approach can address the aforementioned limitations and facilitates the observation of nuclear localization signals in either single cells or populations (Fig. 3A, H and S10).

Adherent cells like fibroblasts require a biocompatible surface for spreading (Fig. 2F). Since different bio-functionalized substrates affect cell morphology (Halldorsson et al., 2015; Tehranirokh et al., 2013), we compared the effect of fibronectin (Gomez-Sjoberg et al., 2007), collagen (Wang et al., 2018), bovine serum albumin (BSA) (Chen et al., 2015), and poly-L-lysine (Wu, 2009), on fibroblast culture. Prior to cell

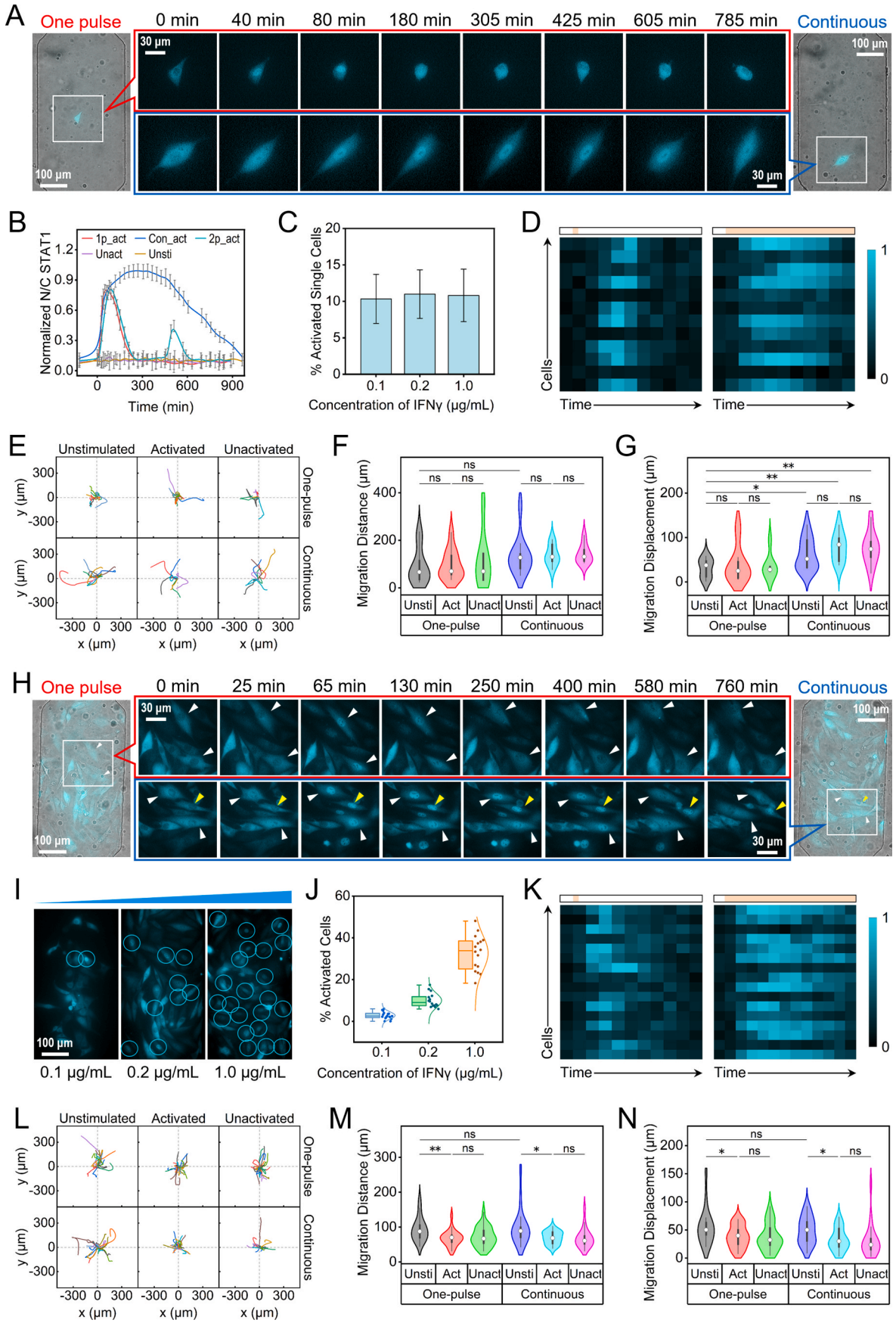

(caption on next page)

Fig. 3. Time-lapse microscopic STAT1 nuclear localization dynamics in (A) isolated single cells or (H) individual cells from a population upon one-pulse or continuous stimulation. (B) Representative dynamic curves of STAT1 activity in isolated single cells treated with IFNγ in a single pulse (10 min), continuous, or two-pulse (10 min for each with 2.5 h interval) manner. 1p_act: activated cell upon one-pulse stimulation. Con_act: activated cell upon continuous stimulation. 2p_act: activated cell upon two-pulse stimulation. Unact: unactivated cell. Unsti: unstimulated cell. The activation rate of (C) isolated single cells or (J) a population over increasing IFNγ dose under one-pulse (10 min) stimulation. (I) Fluorescent images of STAT1 (cyan) nuclear localization in individual cells from a population with increasing concentration of one-pulse (10 min) IFNγ treatment. STAT1 nuclear translocation for distinct IFNγ input dynamics in (D) isolated single cells or (K) populations, with a color gradient from low (black) to high (cyan) representing the ratio of nuclear/cytoplasmic (N/C) fluorescence intensity. The bars above heatmaps depict stimulation profiles such as one 10 min pulse (left) and continuous (right). Representative trajectories of (E) isolated single cells or (L) populations under different stimulation modes. (F, M) Total distance and (G, N) displacement for single-cell or collective cell migration. ns (i.e., not significant): $p > 0.05$, $^{*}p < 0.05$, $^{**}p < 0.01$. Data are representative of three independent experiments. Unsti: unstimulated, Act: activated, Unact: unactivated.

seeding, 100 μg/mL of each coating was perfused into each device. We observed that fibronectin functionalization contributed to fastest cell stretching (Fig. 2G), indicating the best biocompatibility of fibronectin for fibroblast culture in our device. Since adherent cells can shrink under high pressures in microchannels (Armistead et al., 2019; Li et al., 2019), the influence of pressure on fibroblasts was observed (Fig. 2H). Furthermore, the cell stretching rate and morphology were evaluated (Fig. 3I and J). It showed markedly that 1.0 kPa was the best pressure for medium or stimulus delivery.

2.2. Application of the microfluidic approach on integrated analysis of IFNγ-induced homocellular (single-cell, population) STAT1 signaling and migration dynamics

With one-pulse or continuous (i.e., the chambers were kept being flushed with IFNγ) stimulation, we validated the STAT1 activation in isolated single fibroblasts or populations in response to temporal IFNγ (1.0 μg/mL) inputs. The transient STAT1 nuclear localization was observed under each input profile (Fig. 3A and H), which is consistent with a typical STAT1 response in conventional experiments (McBride et al., 2000; Sadzak et al., 2008). Applying two-pulse (10 min for each with 2.5 h interval) IFNγ (1.0 μg/mL) stimulation, STAT1 was reactivated in isolated single cells after a sharp decline in STAT1 activation (Figs. 3B and S11). These results confirm that STAT1 activation can be temporally modulated by introducing temporal stimulation profiles.

The influence of IFNγ dose on STAT1 activation was compared between isolated single cells and populations. Intriguingly, the gradient IFNγ doses did not change STAT1 activation rate in isolated single cells (Fig. 3C), indicating that single-cell STAT1 activation is IFNγ dose-independent. However, STAT1 was activated in only a fraction of cells of the populations with more cells responding at higher IFNγ doses (Fig. 3I and J). This suggests that a population processed analogue IFNγ information but created a digital STAT1 output (Fig. S13), as similarly observed in NF-κB activation in response to tumour-necrosis factor α (TNFα) (Tay et al., 2010). This also implies that cellular communication probably interfered with STAT1 activation at the population level.

Furthermore, we observed distinct STAT1 activation dynamics between one-pulse (10 min) and continuous IFNγ (1 μg/mL) treatment (Fig. 3A and H). To quantify the activation process, STAT1 nuclear/cytoplasmic (N/C) ratios were plotted as heatmaps (Fig. 3D and K). As expected, heterogeneous STAT1 dynamics was observed, demonstrating substantial cell-to-cell variability in IFNγ signal transduction, as similarly found in LPS-induced NF-κB dynamic responses (Junkin et al., 2016; Lee et al., 2014). Overall, both single cells and populations showed more prolonged STAT1 activation under continuous IFNγ exposure compared to one-pulse treatment. These results imply that sustained IFNγ exposure to cells extended working period of STAT1 protein in the nucleus for activating IFN-stimulated genes (Michalska et al., 2018).

Although similar studies (e.g., NF-κB dynamics) have been achieved in different microfluidic designs, it requires either narrow channels with pillar-like traps to isolate single cells (Junkin et al., 2016), or large chambers to observe cell populations (Kellogg et al., 2014). It is challenging to implement both applications in one single device due to the difficulty of integrating two structure designs that differ greatly in size. Moreover, the effect of shear stress on cells could be largely different in these two device designs, which may cause different cellular responses. According to recent studies, TNFα signaling in endothelial cells is shear stress-dependent, resulting in either induction or inhibition of NF-κB activation (Cicha et al., 2009; Ward et al., 2020). Therefore, our approach can address these limitations, thereby providing a general strategy to analyze cellular signaling dynamics at the single-cell or population level on a single platform.

We also investigated the influence of the aforementioned IFNγ treatment (one-pulse or continuous) on the motility of single cells or populations. By measuring cell migration trajectories (Fig. 3E and L), we display violin plots showing total distance (path length), displacement (the absolute distance between cell location at the beginning and the end of tracking), and straightness (calculated by dividing the displacement by the total distance) of fibroblasts subjected to different IFNγ exposures (Fig. 3F, G, M, N and S14). Surprisingly, no significant difference was observed in the straightness between each group of either single cells or populations (Fig. S14). However, the total distance and the displacement both decreased in cell populations with either one-pulse or continuous IFNγ treatment (Fig. 3M and N) but did not change in the IFNγ-stimulated single cells, significantly (Fig. 3F and G). These results indicate that IFNγ inhibited population migration but did not affect single-cell motility. Transforming growth factor β (TGFβ) was previously reported to mediate collective fibroblast migration (Acharya et al., 2008). Since TGFβ signaling was suppressed by IFNγ (Ulloa et al., 1999), the decreases in total distance and displacement were consequently observed in cell populations. Nevertheless, single-cell migration was not affected by IFNγ, indicating a possible co-regulation mechanism rather than mono-regulation by TGFβ. Coupled with immunofluorescence in situ hybridization, more in-depth investigation would be conducted to uncover the important biological mechanisms.

2.3. Application of the microfluidic approach on integrated analysis of LPS-stimulated heterocellular STAT1/2 signaling and migration dynamics

Macrophages and fibroblasts engage in direct communication in the steady state (Franklin, 2021), during fibrosis (Vasse et al., 2021), or within the tumor microenvironment (Gunaydin, 2021). Macrophage-fibroblast communication circuits provide a framework to measure potential outcomes of interacting cells. This facilitates the understanding of the mechanisms underlying macrophage-fibroblast interactions in health, fibrosis, and cancer (Buechler et al., 2021). With our microfluidic system, we can establish a macrophage-to-fibroblast circuit to observe fibroblast response to paracrine mediators from temporally stimulated macrophages (Fig. 1E and H). In order to achieve one-way communication (Fig. 4A), the fibroblasts we used are not able to respond LPS due to their low level of toll-like receptor (TLR4) expression. Since macrophage-fibroblast communication is primarily based on mediator diffusion, we maintained the cocultures in a flow-free environment to prevent any active fluid flow that may influence heterocellular communication or flush away signaling mediators. With the introduction of a 30 min pulse stimulation of 1 μg/mL LPS, transient STAT1 and STAT2 nuclear localization was observed in co-cultured fibroblasts (Fig. 4C and D), indicating STAT1 and STAT2 activation. In accordance to previous studies reporting IFNβ secretion by

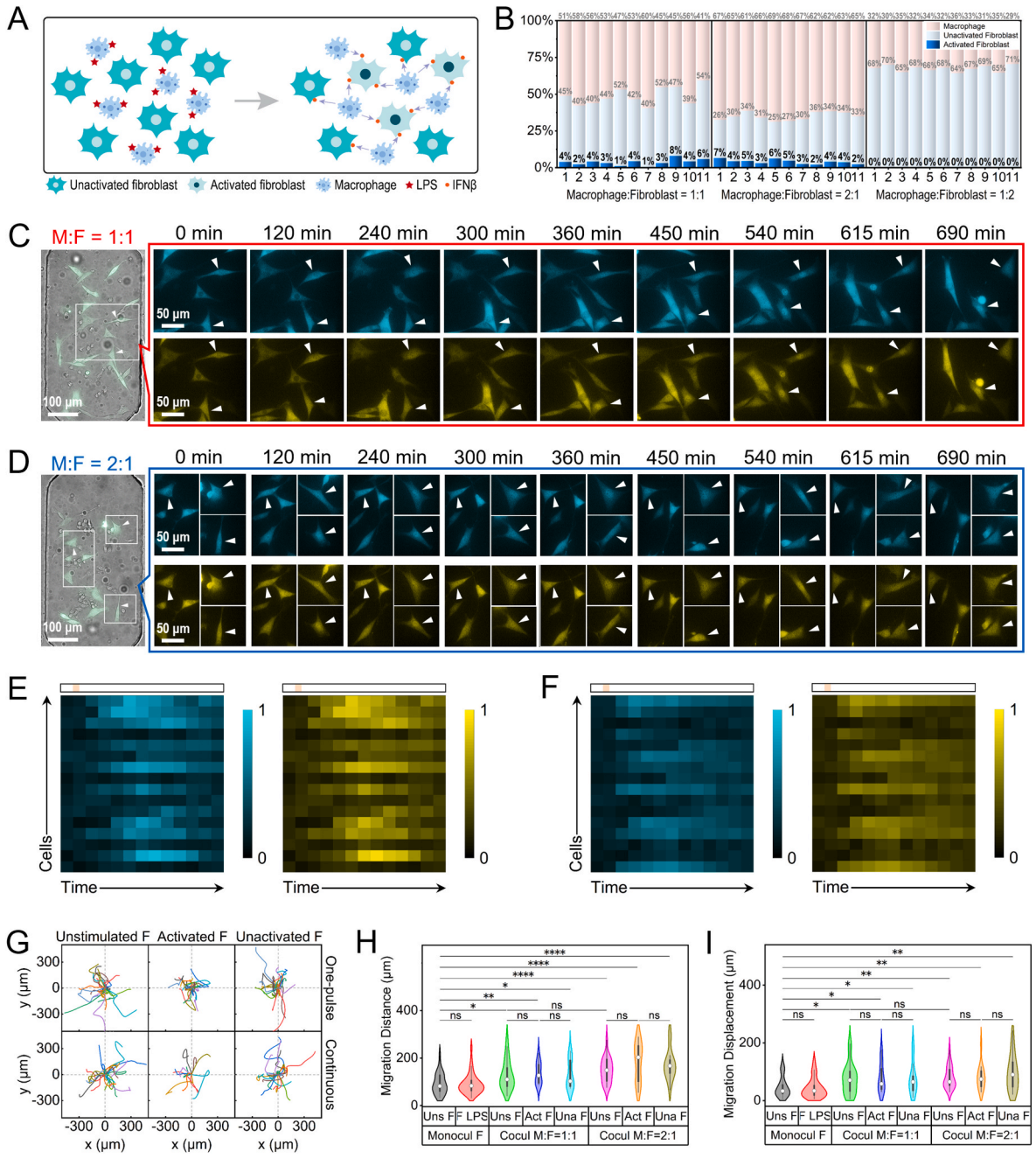

Fig. 4. (A) Schematic of heterocellular signaling by showing macrophages transmitting LPS input to fibroblasts via mediator (i.e., IFNβ) secretion. The fibroblast activation (depicted as nuclear localization signal) is initiated in a digital manner. (B) The proportion of the activated, unactivated fibroblasts, and macrophages from coculture in each chamber (1–11). Time-lapse microscopic STAT1 (cyan) and STAT2 (yellow) dynamics in individual fibroblasts from the coculture at a M:F ratio (C) 1:1 or (D) 2:1. One 30 min pulse of LPS was supplied to the coculture. STAT1 nuclear translocation for diverse IFNγ input dynamics in fibroblasts from the coculture at M:F ratios (E) 1:1 or (F) 2:1. The color bar shows a color gradient from low (black) to high (cyan or yellow) representing STAT1 or STAT2 N/C ratio. The bar above each heatmap depicts a 30 min pulse stimulation profile. (G) Representative trajectories of the cocultured fibroblasts under one-pulse (30 min) stimulation. (H) Total distance and (I) displacement for migration of monocultured or cocultured fibroblasts. ns (i.e., not significant): $p > 0.05$, $^{*}p < 0.05$, $^{**}p < 0.01$. Data are representative of three independent experiments. F: fibroblasts, Uns: unstimulated, F LPS: fibroblasts treated with LPS, Act: activated, Una: unactivated, Monocul: monocultured, Cocul: cocultured.

LPS-stimulated RAW264.7 macrophages (Jacobs and Ignarro, 2001), these results confirm that STAT1 and STAT2 signaling were triggered by paracrine IFNβ mediators.

Other microfluidic coculture systems were applied to study NF-κB activation dynamics in NIH3T3 or HEK293 cells exposed to RAW264.7 macrophage-derived TNFα (Byrne et al., 2014; Frank and Tay, 2015). One-dimensional (1D) mediator diffusion mediated cell-to-cell communication. In contrast, our system allows observation of transcription factor activity in cells encoding two-dimensional (2D) gradients of mediator propagation.

We further explored the influence of coculture ratio on fibroblast activation rate. The coculture at each different macrophage:fibroblast (M:F) ratio (i.e., M:F = 1:2, 1:1 or 2:1) was treated with a 30 min pulse of LPS (1 μg/mL). Surprisingly, STAT1 and STAT2 activation was observed in a small fraction of the co-cultured fibroblasts at 1:1 and 2:1 ratios but not in those at a 1:2 ratio (Figs. 4B and S15). These results indicate both

STAT1 and STAT2 were activated in a digital manner, as similarly observed in IFNγ-induced STAT1 activation. A possible reason for the absence of responding fibroblasts in the coculture at a 1:2 ratio could be insufficient IFNβ secretion by the limited number of macrophages. A huge variation in STAT1 and STAT2 dynamics shown in Fig. 4E and F was likely due to the nonuniform distribution of IFNβ secreted by the macrophages. This implies that the macrophages converted a homogeneous global LPS input into an inhomogeneous localized IFNβ mediator. Overall, the co-cultured fibroblasts at a 1:1 ratio showed stronger peaks in STAT1 and STAT2 dynamics than those at a 2:1 ratio. This is possibly because the macrophages also consumed the mediator, resulting in lower availability for the fibroblasts. Noticeably, long duration of STAT1 and STAT2 activation could be attributed to the sustained IFNβ secretion by the macrophages.

Furthermore, we measured the migration trajectories of individual fibroblasts from either the monoculture or coculture treated with a 30 min pulse of 1 μg/mL LPS (Figs. 4G and S16). As similarly found in single cells or populations, the straightness was not significantly different between the monocultured and cocultured fibroblasts at either a ratio 1:1 or 2:1 (Fig. S17). In addition, LPS treatment had no impact on the motility of monocultured fibroblasts (Fig. 4H, I and S17), suggesting the absence of TLR4 could block the encoding of LPS input and consequently did not affect the regulation of cell migration by TGFβ (Acharya et al., 2008). Overall, the cocultured fibroblasts at either a ratio 1:1 or 2:1 showed a significant increase in the total distance and displacement compared to monocultured cells. Moreover, the fibroblasts enhanced their migration in a coculture environment even without LPS. This indicates that TGFβ signaling might not be disturbed by IFNβ mediator but rather by some other factor arising from the coculture. Although the mechanisms for cell migration were not verified, it would be sufficient to interpret our approach in this application.

3. Conclusion

In summary, we described a universal microfluidic strategy, allowing to confine single cells, populations or cocultures in one single device. This is thus highly applicable for multi-perspective study of cellular signaling and migration behavior in multiple cellular contexts. With temporal input (IFN or LPS) profiles, we demonstrate distinct STAT activities and corresponding migration behaviors of fibroblasts in the aforementioned cellular contexts. Further improvement on automation of bidirectional controllability will simplify handling of single cell seeding. The implementation of other input profiles, such as ramping (Mokashi et al., 2019; Son et al., 2021), would gain more insights into temporal cellular responses in our future work.

CRediT authorship contribution statement

Haowen Yang: Conceptualization, Methodology, Investigation, Data curation, Formal analysis, Visualization, Validation, Project administration, Writing – original draft, Writing – review & editing. **Nidhi Sinha:** Methodology, Software, Writing – review & editing. **Ulfert Rand:** Resources. **Hansjörg Hauser:** Resources. **Mario Köster:** Resources. **Tom F.A. de Greef:** Resources, Writing – review & editing. **Jurjen Tel:** Conceptualization, Project administration, Supervision, Funding acquisition, Writing – review & editing.

Declaration of competing interest

The authors declare that they have no known competing financial interests or personal relationships that could have appeared to influence the work reported in this paper.

Acknowledgements

This result is part of a project, ImmunoCode, that has received funding from the European Research Council (ERC) under the European Union's Horizon 2020 research and innovation programme (Grant agreement No. 802791). Furthermore, we acknowledge generous support by the Eindhoven University of Technology.

Appendix B. Supplementary data

Supplementary data to this article can be found online at https://doi.org/10.1016/j.bios.2022.114353.

References

Acharya, P.S., Majumdar, S., Jacob, M., Hayden, J., Mrass, P., Weninger, W., Assoian, R. K., Pure, E., 2008. J. Cell Sci. 121 (9), 1393–1402.
Armistead, F.J., Gala De Pablo, J., Gadelha, H., Peyman, S.A., Evans, S.D., 2019. Biophys. J. 116 (6), 1127–1135.
Bennett, M.R., Hasty, J., 2009. Nat. Rev. Genet. 10 (9), 628–638.
Buechler, M.B., Fu, W.X., Turley, S.J., 2021. Immunity 54 (5), 903–915.
Byrne, M.B., Trump, L., Desai, A.V., Schook, L.B., Gaskins, H.R., Kenis, P.J.A., 2014. Biomicrofluidics 8 (4).
Chen, H.Y., Sun, J., Wolvetang, E., Cooper-White, J., 2015. Lab Chip 15 (4), 1072–1083.
Cicha, I., Beronov, K., Ramirez, E.L., Osterode, K., Goppelt-Struebe, M., Raaz, D., Yilmaz, A., Daniel, W.G., Garlichs, C.D., 2009. Atherosclerosis 207 (1), 93–102.
Dorrington, M.G., Fraser, I.D.C., 2019. Front. Immunol. 10.
Frank, T., Tay, S., 2015. Lab Chip 15 (10), 2192–2200.
Franklin, R.A., 2021. Immunol. Rev. 302 (1), 86–103.
Gomez-Sjoberg, R., Leyrat, A.A., Pirone, D.M., Chen, C.S., Quake, S.R., 2007. Anal. Chem. 79 (22), 8557–8563.
Gunaydin, G., 2021. Front. Oncol. 11.
Halldorsson, S., Lucumi, E., Gomez-Sjoberg, R., Fleming, R.M.T., 2015. Biosens. Bioelectron. 63, 218–231.
He, C.K., Chen, Y.W., Wang, S.H., Hsu, C.H., 2019. Lab Chip 19 (8), 1370–1377.
Holt, D.J., Chamberlain, L.M., Grainger, D.W., 2010. Biomaterials 31 (36), 9382–9394.
Hong, S., Pan, Q., Lee, L.P., 2012. Integr. Biol.-U.K. 4 (4), 374–380.
Jacobs, A.T., Ignarro, L.J., 2001. J. Biol. Chem. 276 (51), 47950–47957.
Junkin, M., Kaestli, A.J., Cheng, Z., Jordi, C., Albayrak, C., Hoffmann, A., Tay, S., 2016. Cell Rep. 15 (2), 411–422.
Junkin, M., Tay, S., 2014. Lab Chip 14 (7), 1246–1260.
Kellogg, R.A., Gomez-Sjoberg, R., Leyrat, A.A., Tay, S., 2014. Nat. Protoc. 9 (7), 1713–1726.
Lavoie, H., Gagnon, J., Therrien, M., 2020. Nat. Rev. Mol. Cell Biol. 21 (10), 607–632.
Lee, R.E.C., Walker, S.R., Savery, K., Frank, D.A., Gaudet, S., 2014. Mol. Cell. 53 (6), 867–879.
Li, W.W., Mao, S.F., Khan, M., Zhang, Q., Huang, Q.S., Feng, S., Lin, J.M., 2019. ACS Sens. 4 (6), 1710–1715.
McBride, K.M., McDonald, C., Reich, N.C., 2000. EMBO J. 19 (22), 6196–6206.
Michalska, A., Blaszczyk, K., Wesoly, J., Bluyssen, H.A.R., 2018. Front. Immunol. 9.
Mokashi, C.S., Schipper, D.L., Qasaimeh, M.A., Lee, R.E.C., 2019. iScience 19, 586–596.
Osborn, O., Olefsky, J.M., 2012. Nat. Med. 18 (3), 363–374.
Oyler-Yaniv, A., Oyler-Yaniv, J., Whitlock, B.M., Liu, Z.D., Germain, R.N., Huse, M., Altan-Bonnet, G., Krichevsky, O., 2017. Immunity 46 (4), 609–620.
Pang, L., Ding, J., Liu, X.X., Yuan, H.Y., Ge, Y.X., Fan, J.L., Fan, S.K., 2020. TrAC Trends Anal. Chem. (Reference Ed.) 129.
Purvis, J.E., Lahav, G., 2013. Cell 152 (5), 945–956.
Rho, H.S., Yang, Y., Hanke, A.T., Ottens, M., Terstappen, L.W.M.M., Gardeniers, H., 2016. Lab Chip 16 (2), 305–311.
Rothbauer, M., Zirath, H., Ertl, P., 2018. Lab Chip 18 (2), 249–270.
Sadzak, I., Schiff, M., Gattermeier, I., Glinitzer, R., Sauer, I., Saalmuller, A., Yang, E., Schaljo, B., Kovarik, P., 2008. Proc. Natl. Acad. Sci. U.S.A. 105 (26), 8944–8949.
Sakthivel, K., O'Brien, A., Kim, K., Hoorfar, M., 2019. TrAC Trends Anal. Chem. (Reference Ed.) 117, 166–185.
Son, M.J., Wang, A.G., Tu, H.L., Metzig, M.O., Patel, P., Husain, K., Lin, J., Murugan, A., Hoffmann, A., Tay, S., 2021. Sci. Signal. 14 (666).
Spiller, D.G., Wood, C.D., Rand, D.A., White, M.R.H., 2010. Nature 465 (7299), 736–745.
Tape, C.J., 2016. Trends Biotechnol. 34 (8), 627–637.
Tay, S., Hughey, J.J., Lee, T.K., Lipniacki, T., Quake, S.R., Covert, M.W., 2010. Nature 466 (7303), 267. U149.
Tehranirokh, M., Kouzani, A.Z., Francis, P.S., Kanwar, J.R., 2013. Biomicrofluidics 7 (5).
Ulloa, L., Doody, J., Massague, J., 1999. Nature 397 (6721), 710–713.
Vasse, G.F., Nizamoglu, M., Heijink, I.H., Schleputz, M., van Rijn, P., Thomas, M.J., Burgess, J.K., Melgert, B.N., 2021. J. Pathol. 254 (4), 344–357.
Villarino, A.V., Kanno, Y., O'Shea, J.J., 2017. Nat. Immunol. 18 (4), 374–384.
Vu, T.Q., de Castro, R.M.B., Qin, L.D., 2017. Lab Chip 17 (6), 1009–1023.
Wang, C.Y., Tanataweethum, N., Karnik, S., Bhushan, A., 2018. ACS Biomater. Sci. Eng. 4 (4), 1377–1385.
Ward, A.O., Angelini, G.D., Caputo, M., Evans, P.C., Johnson, J.L., Suleiman, M.S., Tulloh, R.M., George, S.J., Zakkar, M., 2020. Sci. Rep.-U.K. 10 (1).
Wells, A., Wiley, H.S., 2018. Essays Biochem. 62 (4), 607–617.
Wimmers, F., Subedi, N., van Buuringen, N., Heister, D., Vivie, J., Beeren-Reinieren, I., Woestenenk, R., Dolstra, H., Piruska, A., Jacobs, J.F.M., van Oudenaarden, A., Figdor, C.G., Huck, W.T.S., de Vries, I.J.M., Tel, J., 2018. Nat. Commun. 9.
Wu, M.H., 2009. Surf. Interface Anal. 41 (1), 11–16.